

## Objective Identification of Annular Hurricanes

JOHN A. KNAFF

*NOAA/NESDIS/Center for Satellite Applications and Research, Fort Collins, Colorado*

THOMAS A. CRAM

*Department of Atmospheric Science, Colorado State University, Fort Collins, Colorado*

ANDREA B. SCHUMACHER

*Cooperative Institute for Research in the Atmosphere, Colorado State University, Fort Collins, Colorado*

JAMES P. KOSSIN

*Cooperative Institute for Meteorological Satellite Studies, University of Wisconsin—Madison, Madison, Wisconsin*

MARK DEMARIA

*NOAA/NESDIS/Center for Satellite Applications and Research, Fort Collins, Colorado*

(Manuscript received 26 March 2006, in final form 21 June 2007)

### ABSTRACT

Annular hurricanes are a subset of intense tropical cyclones that have been shown in previous work to be significantly stronger, to maintain their peak intensities longer, and to weaken more slowly than average tropical cyclones. Because of these characteristics, they represent a significant forecasting challenge. This paper updates the list of annular hurricanes to encompass the years 1995–2006 in both the North Atlantic and eastern–central North Pacific tropical cyclone basins. Because annular hurricanes have a unique appearance in infrared satellite imagery, and form in a specific set of environmental conditions, an objective real-time method of identifying these hurricanes is developed. However, since the occurrence of annular hurricanes is rare (~4% of all hurricanes), a special algorithm to detect annular hurricanes is developed that employs two steps to identify the candidates: 1) prescreening the data and 2) applying a linear discriminant analysis. This algorithm is trained using a dependent dataset (1995–2003) that includes 11 annular hurricanes. The resulting algorithm is then independently tested using datasets from the years 2004–06, which contained an additional three annular hurricanes. Results indicate that the algorithm is able to discriminate annular hurricanes from tropical cyclones with intensities greater than 84 kt ( $43.2 \text{ m s}^{-1}$ ). The probability of detection or hit rate produced by this scheme is shown to be ~96% with a false alarm rate of ~6%, based on 1363 six-hour time periods with a tropical cyclone with an intensity greater than 84 kt (1995–2006).

### 1. Introduction

A subset of tropical cyclones, referred to as annular hurricanes, were introduced and diagnosed in an observational study (Knaff et al. 2003, hereafter K03). An

annular hurricane (AH), as observed in infrared (IR) imagery, has a larger-than-average size eye, symmetrically distributed cold brightness temperatures associated with eyewall convection, and few or no rainband features. K03 used these features to subjectively identify six AHs in the Atlantic and eastern–central North Pacific tropical cyclone basins. Findings of K03 show that AH formation was systematic, resulting from what appeared to be asymmetric mixing of eye and eyewall components of the storms that involved one or two possible mesovortices—a contention supported by limited aircraft reconnaissance data and satellite imagery.

---

*Corresponding author address:* John Knaff, NOAA/NESDIS/Office of Research and Applications, CIRA/Colorado State University, Foothills Campus Delivery 1375, Fort Collins, CO 80523-1375.

E-mail: john.knaff@noaa.gov

The AHs were also shown to exist and develop in specific environmental conditions that are characterized by 1) relatively weak easterly or southeasterly vertical wind shear, 2) easterly winds and colder-than-average temperatures at 200 hPa, 3) a specific range (25.4°–28.5°C) of sea surface temperatures (SSTs) with small variations along the storm track, and 4) a lack of 200-hPa relative eddy flux convergence due to interactions with the environmental flow. Weak easterly shear is hypothesized to promote the symmetric nature of AHs by canceling the effect of vertical wind shear induced by the vortex interacting with gradients of planetary vorticity. With respect to maximum wind speed, AHs were significantly stronger, maintained their peak intensities longer, and weakened more slowly, than the average tropical cyclone in these basins (see Fig. 3 in K03). As a result, average official forecast intensity errors for these types of tropical cyclones were 10%–30% larger than the 5-yr (1995–99) mean official errors during the same period with pronounced negative biases (e.g., –17.1 kt for the 48-h forecast).

Since the formal documentation of AHs, also referred to as “truck tire” or “doughnut” tropical cyclones by some forecasters, there have been a few idealized numerical modeling studies that examine the combined effect of environmental and beta-vortex-induced shear or “beta shear.” The beta shear results from the differential advection of planetary vorticity within the tropical cyclone with height and weakening of the beta gyres (Chan and Williams 1987; Fiorino and Elsberry 1989) as a result of the cyclone’s warm core structure (Wang and Holland 1996a,b,c; Bender 1997; Peng et al. 1999; Wu and Braun 2004; Ritchie and Frank 2007). The majority of previous idealized numerical studies of tropical cyclones were conducted on an  $f$  plane, primarily to keep the influence of planetary vorticity and its influences on motion and vertical wind shear separate from other processes of interest. In general,  $f$ -plane simulations result in quite symmetric simulated tropical cyclones in the absence of vertical wind shear, but the occurrence or development of AH-type structures (i.e., symmetric with a large, temporally invariant radius of maximum winds) to our knowledge has not been explicitly reported or examined. However, it has been established that rather small magnitudes ( $< \sim 3 \text{ m s}^{-1}$ ) of vertical wind shear lead to convective asymmetries and corresponding weakening of the vortex in such simulations (e.g., Ritchie and Frank 2007).

Recently, there has been renewed interest in the effect of the advection of planetary vorticity on the evolution of tropical cyclone structure. The inclusion of these effects, in an environment at rest, has also produced a more asymmetric and slightly larger tropical

cyclone that intensifies slightly slower than its  $f$ -plane counterpart in terms of minimum sea level pressure (MSLP) (Ritchie and Frank 2007). Wu and Braun (2004) produced similar results in tropical cyclone simulations where the inclusion of beta shear results in more asymmetries and a weaker tropical cyclone. In another study, Kwok and Chan (2005) found that uniform westerly steering flow in variable- $f$  simulations partially cancels the beta shear, while easterly uniform steering flow enhances it—findings that confirm earlier results presented in Peng et al. (1999). The greater asymmetry in tropical cyclone (TC) structure in these TC simulations is in a large part due to the vertical wind shear variations that result from the inclusion of the planetary vorticity advection. Simulations of tropical cyclones using environmental conditions similar to those documented in K03 have also been shown to result in a more axisymmetric tropical cyclone (Ritchie 2004). One can interpret these results as implying that beta shear in these simulations produces greater TC asymmetries, and if the environmental wind shear opposes the beta shear, these asymmetries are reduced. Furthermore, if the environmental conditions nearly cancel the beta shear, the TC can be axisymmetric, which supports the suggestions made in K03 that *annular hurricanes form in environments where the environmental vertical wind shear nearly cancels the beta shear and further intensification is limited by less than ideal thermodynamic conditions (i.e., atypically low SSTs conditions)*.

AHs are intense tropical cyclones with average intensities greater than 100 kt (or  $51 \text{ m s}^{-1}$ )—major hurricanes, and, despite their less-than-optimal thermodynamic conditions (i.e.,  $\text{SSTs} \leq \sim 28.5^\circ\text{C}$ ), they maintain intensities close to their maximum potential intensity with respect to SST (e.g., DeMaria and Kaplan 1994b). Because of this intensity change behavior, intensities of past AHs have been consistently underforecast. The mean intensity of AHs makes them potentially high-impact events when they affect coastal areas. Objective identification of AHs in an operational setting could help forecasters better predict future intensity changes for these tropical cyclones, and likely reduce the overall intensity forecast errors. This could be accomplished by subjectively forecasting slower weakening or no weakening while AH conditions exist. K03 recognized the need for better identification of AHs and suggested methods that used environmental conditions and IR imagery separately to identify, in a dependent manner, the six AHs that occurred in the Atlantic and eastern-central North Pacific during 1995–99. This paper expands on those ideas and the results of recent modeling studies to create a method to objectively identify AHs.

This objective method, which uses information about the storm's environmental conditions, intensity, and appearance in IR satellite imagery, is described in the following sections.

## 2. Data and approach

In K03 the developmental data for the Statistical Hurricane Intensity Prediction Scheme (SHIPS; DeMaria and Kaplan 1994a, 1999; DeMaria et al. 2005) were used to determine the environmental conditions associated with AHs. Following the logic of K03, the SHIPS developmental data (SDD) are used in a similar way in this study, but the calculations used to create the SDD have continued to evolve. The largest changes to the SDD involve how vertical wind shear was calculated. The vertical shear calculation used in K03 was averaged in a circular area within a radius of 600 km following a Laplacian filtering procedure that was used to remove the effects of the TC vortex as described in DeMaria and Kaplan (1999). In the current version of SDD, no attempt is made to remove the storm vortex and an annular average (200–800 km) is used to estimate the environmental vertical wind shear. The current SDD also uses the National Centers for Environmental Prediction–National Center for Atmospheric Research (NCEP–NCAR) reanalyses (Kalnay et al. 1996) prior to 2001 and the NCEP Global Forecast System (GFS; Lord 1993) analyses thereafter. SST estimates are still estimated from Reynolds's (1988) weekly SST fields. The position of the tropical cyclone and its intensity come from the National Hurricane Center (NHC) best track (Jarvinen et al. 1984). Note that because tropical cyclone intensity is reported and archived in units of knots (kt;  $1 \text{ kt} = 0.51 \text{ m s}^{-1}$ ), this unit will be used for intensity throughout this manuscript. Because of these changes, the latest version of the SDD (see DeMaria et al. 2005) at 6-h intervals for 1995–2006 is used for this study, where the period 1995–2003 is used as a dependent dataset and 2004–06 are retained for independent testing.

In addition to the SDD, Geostationary Operational Environmental Satellite (GOES) IR imagery with wavelengths centered near  $10.7 \mu\text{m}$  is used in the form of 4-km Mercator projections during the period 1995–2006. The GOES IR imagery is taken from the Cooperative Institute for Research in the Atmosphere (CIRA) Tropical Cyclone IR Archive (Mueller et al. 2006; Kossin et al. 2007). Individual images were renavigated to storm-centric coordinates using cubic-spline interpolated best-track positions (Kossin 2002). The time interval between images is generally 30 min, with the exception of the satellite “eclipse” periods oc-

curing within approximately a month of the autumnal equinox and the last 1–3 h. In this study IR brightness temperature ( $T_B$ ) is azimuthally averaged about the storm center and time averaged over a 6-h time period, corresponding to the 6 h prior to the analysis time. This time interval corresponds to the times in the NHC best track and the times in SDD. Figure 1 shows an IR image of eastern North Pacific Hurricane Daniel on 27 July 2001 at 2200 UTC, and the corresponding radial profiles azimuthal mean and standard deviation of  $T_B$ . Some of the characteristics of annular hurricanes can be quantified directly from these data (e.g., the existence of large warm eye features or the relative lack of rain-band activity).

Changes in how environmental conditions have been derived in the updated SDD require that the statistics of the environmental conditions associated with the original six AHs be recalculated. Using the most recent SDD and the IR image archive, statistics of key environmental conditions and IR imagery characteristics associated with the six AHs described in K03 are shown in Table 1. Thirty-six 6-h time periods make up each average. The average quantities calculated from the IR imagery and shown in Table 1 include the radius of coldest azimuthally averaged  $T_B$  ( $R_c$ ) as illustrated in Fig. 1, the azimuthal standard deviation at  $R_c$  ( $\sigma_c$ ) also shown in Fig. 1, the variance of the azimuthally averaged temperatures from the TC center to 600 km (VAR), and the maximum difference between  $T_B$  at  $R_c$  and any azimuthally averaged  $T_B$  at smaller radii ( $\Delta T_{\text{eye}}$ ). Table 1 also includes the statistics associated with the SSTs interpolated to the TC center (SST), the magnitude of the 200–850-hPa wind shear vector (SHRD), the magnitude of the 500–850-hPa wind shear (SHRS) vector, the zonal wind component at 200 hPa (U200), the temperature at 200 hPa (T200), the relative eddy flux convergence (REFC; see K03), and the best-track value of maximum wind speed ( $V_{\text{max}}$ ). The SHRD, SHRS, U200, and T200 parameters were calculated in a 200–800-km annulus centered on the TC and the REFC was calculated within 600 km of the TC center as described in DeMaria et al. (2005). These statistics are consistent with the environmental and visual characteristics of annular hurricanes (i.e., K03, their Table 3 and Fig. 7). Small differences do occur due to the differences in how the SDD parameters are calculated, and the use of 6-h versus the 12-h time-averaging periods used in K03. These new statistics are used as a starting point to develop an objective identification technique discussed in the next section.

Since the publication of K03, a few more annular cases have occurred in the Atlantic and eastern North Pacific. There has also been an opportunity to examine

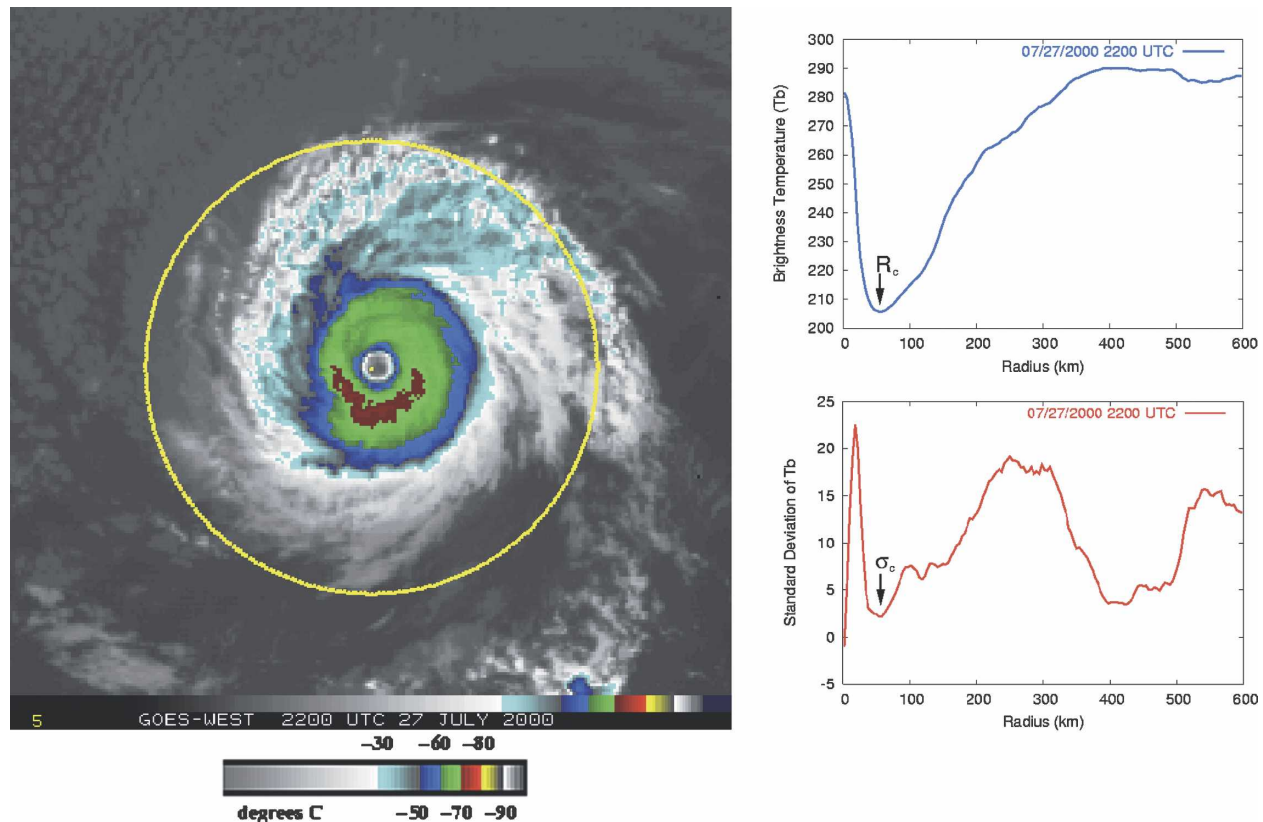


FIG. 1. (left) Storm-centered IR image of east Pacific Hurricane Daniel at 2200 UTC 27 Jul 2000 and (top right) the corresponding radial profiles of azimuthally averaged brightness temperatures with an arrow pointing to the radius of coldest average brightness temperature indicated as  $R_c$  and (bottom right) the azimuthal std devs with an arrow pointing to the value of the std dev at  $R_c$  and identified as  $\sigma_c$ . The yellow circle centered within the image has a radius of 300 km for reference.

some IR imagery prior to 1997 in the eastern Pacific. The expanded list of subjectively identified AHs for the period 1995–2006 is shown in Table 2. Eight cases, several short lived (i.e., Erin in 2001, Kate in 2003, and Frances in 2004 in the Atlantic, and Daniel in 2000 and Bud in 2006 in the eastern Pacific) were added to the list. However, since 2000, there have been a couple of exceptional AH cases. Hurricanes Isabel (2003) and Daniel (2006) were both spectacular examples of AHs. Hurricane Isabel had four distinct periods with AH characteristics, each following a rearrangement of the eye, and Hurricane Daniel (2006) exhibited classic AH formation with eye-to-eyewall mixing, indicated by one or more mesovortices seen in the IR imagery, followed by the formation of a large warm eye and diminished rainband activity that lasted over 30 h.

The GOES IR satellite imagery associated with these 14 subjectively identified AH cases for 1995–2006 (Fig. 2) shows a large variety of sizes. The Atlantic AHs (yellow text), in general, appear larger than the eastern–central North Pacific AHs (cyan text). In fact, the

average 34-kt wind radius is 109 n mi (202 km) and 135 n mi (250 km) for the eastern–central North Pacific and Atlantic cases, respectively. These results are consistent with the tropical cyclone size climatology of these basins (Knaff et al. 2007) and cyclone sizes reported in Knaff and Zehr (2007), where 25 n mi (46 km) separate the average 34-kt wind radius between the East Pacific and Atlantic basins. One could speculate that environmental conditions in the eastern–central North Pacific are less conducive for TC growth because upper-level trough interaction, and extratropical transition, both related to TC growth (Maclay 2006; Maclay et al. 2007, manuscript submitted to *Mon. Wea. Rev.*), occur less frequently in that basin. The average AH intensity is 110 kt ( $56.6 \text{ m s}^{-1}$ ) and ranged from a low of 90 kt ( $46 \text{ m s}^{-1}$ ) to a high of 140 kt ( $72 \text{ m s}^{-1}$ ). From the subjectively determined time periods in Table 2, the average duration of an AH is approximately 18 h with a maximum of 57 h associated with Hurricane Howard in 1999. There also appears to be a preferred climatological time for formation. Eastern–central North Pacific

TABLE 1. Statistics of the important environmental conditions and IR imagery–derived characteristics related to AHs. Statistics are shown for the radius of coldest azimuthally averaged  $T_B$  ( $R_c$ ), the azimuthal standard deviation at  $R_c$  ( $\sigma_c$ ), the variance of the azimuthally averaged temperatures from the TC center to 600 km (VAR), the maximum difference between  $R_c$  and any azimuthally averaged  $T_B$  at smaller radii ( $\Delta T_{\text{eye}}$ ), the SSTs interpolated to the TC center (SST), the magnitude of the 200–850-hPa wind shear vector (SHRD), the magnitude of the 500–850-hPa wind shear (SHRS) vector, the zonal wind component at 200 hPa (U200), the temperature at 200 hPa (T200), the relative eddy flux convergence (REFC), and the best-track value of maximum wind speed ( $V_{\text{max}}$ ).

Quantity (units)	Mean	Std dev	Min	Max
$R_c$ (km)	80.9	19.7	62.0	128.0
$\sigma_c$ ( $^{\circ}\text{C}$ )	3.0	1.1	1.5	5.8
VAR ( $^{\circ}\text{C}^2$ )	712.1	141.3	391.2	978.6
$\Delta T_{\text{eye}}$ ( $^{\circ}\text{C}$ )	69.3	13.5	19.6	79.9
SST ( $^{\circ}\text{C}$ )	26.7	0.7	25.4	28.4
SHRD ( $\text{m s}^{-1}$ )	4.0	1.5	1.2	8.1
SHRS ( $\text{m s}^{-1}$ )	3.2	1.2	0.7	6.0
U200 ( $\text{m s}^{-1}$ )	−4.8	2.3	−7.2	0
T200 ( $^{\circ}\text{C}$ )	−52.2	0.9	−53.4	−50.1
REFC ( $\text{m s}^{-1} \text{ day}^{-1}$ )	0.2	1.2	−4.0	4.0
$V_{\text{max}}$ (kt)	107.2	12.8	85.0	125.0

AHs tend to form from mid-July to late August whereas Atlantic AH occurrence seems to be from mid-August to mid-October. Figure 3 shows the tracks associated with the 14 AHs listed in Table 2. These storms are not typically a threat to the U.S. mainland, but rather may be more of a concern for the Windward, Leeward, and Hawaiian Islands. There appears to be a

preferred location near  $15^{\circ}\text{N}$  and  $125^{\circ}\text{W}$  in the eastern North Pacific while Atlantic AHs show greater variability in their locations. It is also important to note that the inclusion of the new cases does not change the findings of K03 related to AH intensity behavior. The AHs were still found to be significantly stronger, maintained their peak intensities longer, and weakened more slowly than the average of all hurricanes.

### 3. Algorithm development

As described in K03, AHs occur in specific environmental conditions, characterized by a combination of weak easterly or southeasterly vertical wind shear in deep-layer mean easterlies and relatively cold temperatures at 200 hPa, moderate SST, and relatively small 200-hPa relative eddy flux convergence (REFC) due to environmental interactions. The AHs also appear distinctly more axisymmetric in IR satellite imagery with large circular eyes surrounded by a nearly uniform ring of convection and a relative lack of deep convective features, including rainbands outside that ring. From results presented in K03, it also appears that the environmental conditions can be combined with the IR satellite imagery–derived characteristics of AHs to separate the population of annular hurricanes from the larger population of nonannular hurricanes. At first glance, this process would seem straightforward, but AHs are also rare events that occur in less than 4% of all hurricane cases, which makes many standard statistical identification algorithms impractical.

TABLE 2. List of the 14 AH cases identified in the Atlantic and east Pacific Hurricane basins (1995–2006). Listed are the storm, basin, the times associated with the AH phase, the number of hours that each AH phase lasted, and the intensity range associated with the storm.

Storm	Basin	Annular period	Duration (h)	Intensity range (kt)
Luis 1995	Atlantic	1800 UTC 3 Sep–0400 UTC 4 Sep	10	120–125
Edouard 1996	Atlantic	0000 UTC 25 Aug–0000 UTC 26 Aug	24	120–125
Erin 2001	Atlantic	0400 UTC 10 Sep–0900 UTC 10 Sep	6	100–105
Isabel 2003	Atlantic	0700 UTC 11 Sep–2100 UTC 11 Sep	14	135–145
		1000 UTC 12 Sep–2200 UTC 12 Sep	12	140
		1400 UTC 13 Sep–0200 UTC 14 Sep	12	135–140
		0700 UTC 14 Sep–2000 UTC 14 Sep	14	135–140
Kate 2003	Atlantic	1700 UTC 03 Oct–0000 UTC 4 Oct	5	100
		0400 UTC 04 Oct–1300 UTC 4 Oct	10	100–105
Frances 2004	Atlantic	2100 UTC 28 Aug–0200 UTC 29 Aug	6	115
Barbara 1995	East Pacific	0500 UTC 14 Jul–1400 UTC 14 Jul	10	115–120
Darby 1998	East Pacific	1200 UTC 26 Jul–1800 UTC 27 Jul	30	90–100
Howard 1998	East Pacific	1800 UTC 24 Aug–0300 UTC 27 Aug	57	115–85
Beatriz 1999	East Pacific	1800 UTC 12 Jul–1800 UTC 13 July	24	100–105
Dora 1999	East Pacific	1800 UTC 10 Aug–0300 UTC 12 Aug	33	115–120
		0300 UTC 15 Aug–0300 UTC 16 Aug	24	90–95
Daniel 2000	East Pacific	2000 UTC 27 Jul–0400 UTC 28 Jul	9	95
Bud 2006	East Pacific	0700 UTC 13 Jul–1300 UTC 13 Jul	6	100
Daniel 2006	East Pacific	1400 UTC 21 Jul–2200 UTC 22 Jul	33	120–130

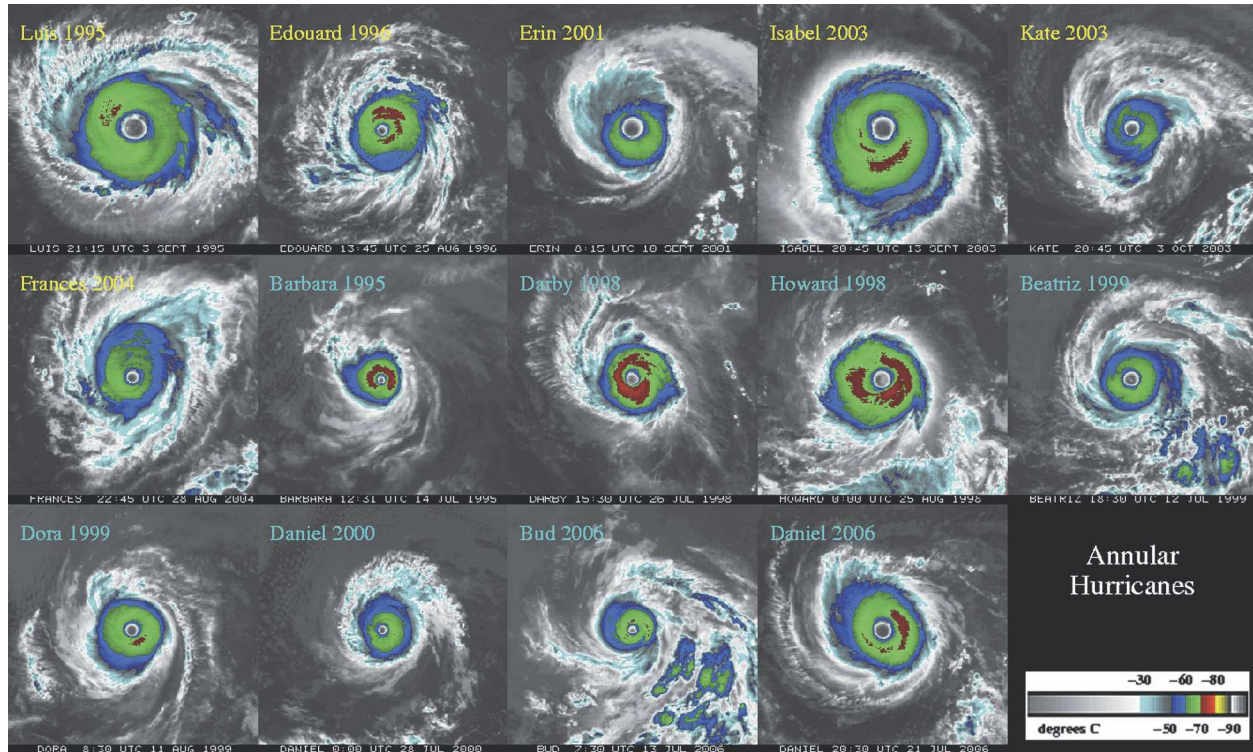


FIG. 2. Color-enhanced GOES IR satellite imagery of the 14 annular hurricane cases at or near peak visual annular characteristics. Storm names, dates, and times are given at the bottom of each individual image panel. In addition, storm names and years are listed in the upper left of each image panel with North Atlantic and eastern-central North Pacific storm names indicated by yellow and cyan text, respectively.

To find the relatively rare occurrences of AHs in the combined Atlantic and eastern-central North Pacific TC sample, a two-step algorithm is developed. The first step is to prescreen the SDD and IR satellite data for cases when the environmental conditions and IR satellite  $T_B$  distribution are unfavorable for AHs. The second step is to apply a statistical technique called linear

discriminant analysis (LDA; see Wilks 2006) to the SSD and IR satellite dataset that remains after the screening step. LDA is a formal technique that discriminates between two or more populations using linear combinations of a set of discriminators. To test the ability of this two-step algorithm to discriminate events from nonevents, we use the hit rate and the false alarm

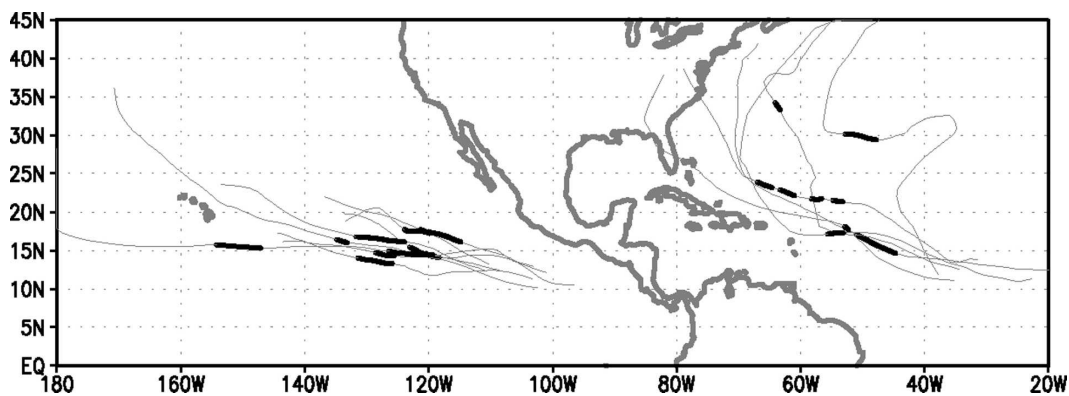


FIG. 3. Map of the tracks of the 14 annular hurricane cases used in this study. The time periods when these hurricanes were subjectively identified to be annular hurricanes are indicated by the thick black portion of the track.



TABLE 3. Summary of selection rules used to prescreen the input data and remove cases when an AH event is unlikely. Variables as in Table 1.

Parameter	Source	Prescreening criterion
$R_c$	IR satellite imagery	<50 km
$\Delta T_{eye}$	IR satellite imagery	<15°C
SHRD	NCEP–NCAR analysis	>11.3 m s <sup>-1</sup>
U200	NCEP–NCAR analysis	<-11.8 or >1.5 m s <sup>-1</sup>
REFC	NCEP–NCAR analysis	<-9 or >11 m s <sup>-1</sup> day <sup>-1</sup>
SST	Reynolds SST	<24.3 or >29.1°C
Intensity	NHC best track	<85 kt

rate (Mason and Graham 1999). The hit rate is the number of correctly identified AH cases divided by the number of AHs observed and the false alarm rate is the number of incorrectly identified AH cases divided by the total number of nonannular hurricane (NAH) cases observed, which for this study includes all storms that passed the screening and were not AHs. One caveat to this study is that the subjectively identified AH cases are used to develop and then independently test this objective technique, which is far from ideal and will likely degrade the final algorithm (section 4).

For the screening step, a set of “selection” rules are determined to eliminate cases where AHs are very unlikely to occur given the environmental conditions and IR characteristics. These criteria are listed in Table 3. To be as inclusive as possible, the environmental discriminators were set to values that capture the 54 six-hour time periods associated with the 11 AHs that occurred during 1995–2003. The thresholds for storm intensity,  $\Delta T_{eye}$  and  $R_c$ , which are far from normally distributed, are set to values slightly less than the minima of the AH sample. The SST is used as another criterion to eliminate NAH cases since AHs are observed to occur in a distinct range of SST values. The SST thresholds are based on the mean  $\pm 3$  standard deviations of the annular group sample. The selection rules were applied to the original data sample (1995–2003) that contained 976 six-hour tropical cyclone cases with intensities greater than 84 kt. After the selection rules were applied, there were 241 remaining 6-h cases, of which 53 were objectively identified and subjectively confirmed as being AHs (1 case was missing quality IR satellite imagery). Thus, the prescreening of the dependent dataset had a 100% hit rate, but a false alarm rate of 19%, given the 972 cases that passed the screening. Using LDA, we hope to improve the false alarm rate.

LDA is then used to take advantage of differences between the AH and NAH samples. From the 1995–2003 cases, the environmental factors that had significant annular versus nonannular differences were used

TABLE 4. Normalized coefficients of the AH discriminant vector based upon the 1995–2002 AH cases. Variables as in Table 1. Note the discriminant divider is a unitless number that causes the discriminant function values to be centered about a zero value.

Discriminator	Mean	Std dev	Normalized coefficient
$\sigma_c$	4.21	2.56	-0.40
VAR	552.73	215.10	0.79
$\Delta T_{eye}$	59.67	20.99	0.50
U200	-3.72	2.88	-0.11
SST	27.58	1.08	-0.61
Discriminant divider			0.53

as discriminators in the LDA. Results show that an environment characterized by lower SSTs and easterly zonal 200-hPa winds and IR imagery depicting warm eyes, a radius of the coldest pixel (i.e., inner-core convection) with little azimuthal variability, and a less variable radial profile of brightness temperatures (i.e., fewer rainbands) form the basis for discriminating AHs from NAHs in the screened sample. The environmental discriminators therefore are 1) SST and 2) U200. Similarly, the IR-based discriminators used are 1)  $\sigma_c$ , 2) VAR, and 3)  $\Delta T_{eye}$ . All of the above discriminators were chosen based on their statistical significance (i.e., exceeding the 95% significance level using a two-tailed Student’s *t* test) between the sample data means of the AH and NAH cases that passed the prescreening process. The storm cases chosen to belong to the group of AHs in the LDA development are the 11 cases with 53 six-hour periods subjectively determined to be AHs listed in Table 1 for the period 1995–2003.

The prescreened data have been normalized prior to carrying out the LDA by subtracting the sample mean and then dividing by the sample standard deviation for each discriminator. Standardizing the input data allows one to estimate the relative importance of each parameter in the LDA. LDA then provides the normalized weights for the linear combination of the input variables that best differentiates between AH and NAH cases. Table 4 shows the normalized discriminant weights produced by the LDA. Also shown in Table 4 are the means and standard deviations associated with the parameter calculated from the 241 prescreened cases, which are used for parameter normalization. When the discriminant vector is applied, positive values are indicative of AHs. Noting that the prescreening requires a large eye and a low vertical shear environment, Table 4 indicates that the largest contribution to the discrimination comes from the factors associated with SST, and VAR (i.e., variance of the radial profile of azimuthal mean brightness temperatures), which is a measure of significant rainband activity.

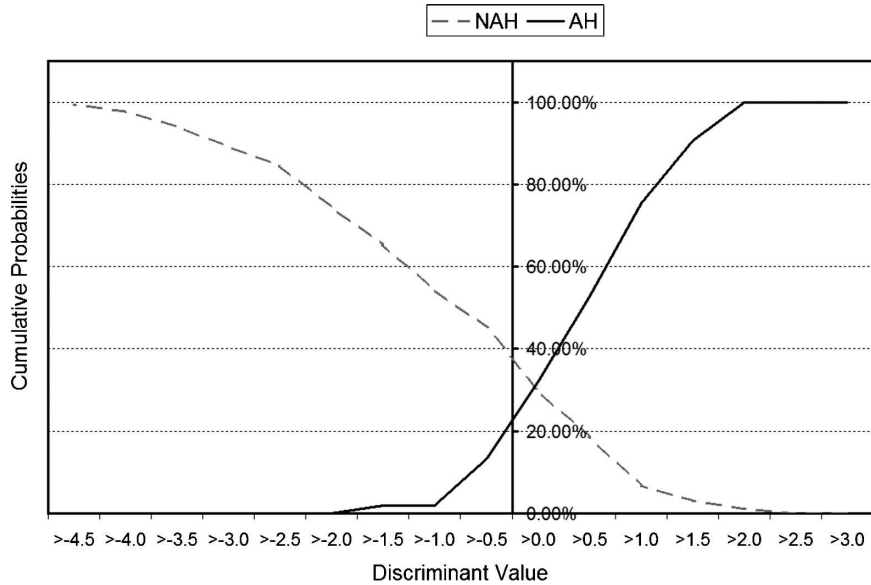


FIG. 4. The cumulative probability distributions associated with the dependent data (1995–2003) as a function of binned discriminant function values created by the LDA. The dashed line is for the NAH cases and the solid line is for the AH cases.

The linear combination of the normalized discriminant weights and the standardized input variables for both AH and NAH cases are then calculated to determine the value of the discriminant function at each analysis time. Although the LDA is designed to produce a yes–no answer, the range of values of the discriminant function performed on the dependent data sample allows us to assign a normalized annular hurricane index value to each case. The relative magnitude of the discriminant value is an indicator of how “annular” a particular case is.

The results from the linear discriminant function, however, are not perfect and misidentified 56 of 188 NAH cases as being annular and 7 of the 53 AH cases as being NAH. Using the dependent sample and combining the two steps (i.e., prescreening and LDA) shows that the algorithm identified 46 of the 53 six-hour periods when AH existed and had a hit rate of 87%, while only falsely identifying 56 cases as AH out of 923 eighty-four-kt or greater 6-h NAH cases resulting in a false alarm rate of ~6%. The seven false negatives occurred with 1) short-lived annular hurricanes (Luis in 1995, Erin in 2001, and Kate in 2003), which accounted for four cases, and 2) cases associated the first 6-h period in the annular phase. These false negative cases had an average discriminant value of 0.39 and only one case (Beatriz) had a value greater than 1.25, which was due to the rapid evolution of Beatriz and the time averaging applied to the IR  $T_B$  data. Most of the false positives were associated with AHs but at times before

or after their subjectively determined annular phase(s). The average of the discriminant value for these 56 cases was  $-0.76$ . Other false positives that were never AHs include the east Pacific Hurricanes Felicia (1997), Guillermo (1997), Georgette (1998), Adolf (2001), Hernan (2002), and Jimena (2003) with two, one, three, one, two, and two 6-hourly time periods misidentified, respectively. Similarly Atlantic Hurricanes Georges (1998), Alberto (2000), Isidore (2000), and Fabian (2003) had two, one, one, and one 6-h time periods that were misidentified, respectively. Figure 4 shows the cumulative probability diagrams for the AH and NAH cases as a function of the discriminant value, which shows the LDA properly discriminating the majority of the cases with a larger probability of false identification than of false alarm rate. For the final algorithm (section 4), it will be desirable to maximize the hit rate while minimizing the false alarms through scaling of the discriminant function values using information in such diagrams.

It is interesting to examine what the LDA is actually discriminating. To briefly show what the LDA algorithm determines as an AH case versus a NAH case, four time periods of Hurricane Isabel with varying degrees of AH characteristics are examined. Figure 5 shows IR imagery of Hurricane Isabel and corresponding discriminant value at 0345 UTC 11 September, 1145 UTC 12 September, 0345 UTC 14 September, and 1145 UTC 18 September. The 0345 UTC time is the last image used for the annular index estimation at 0600



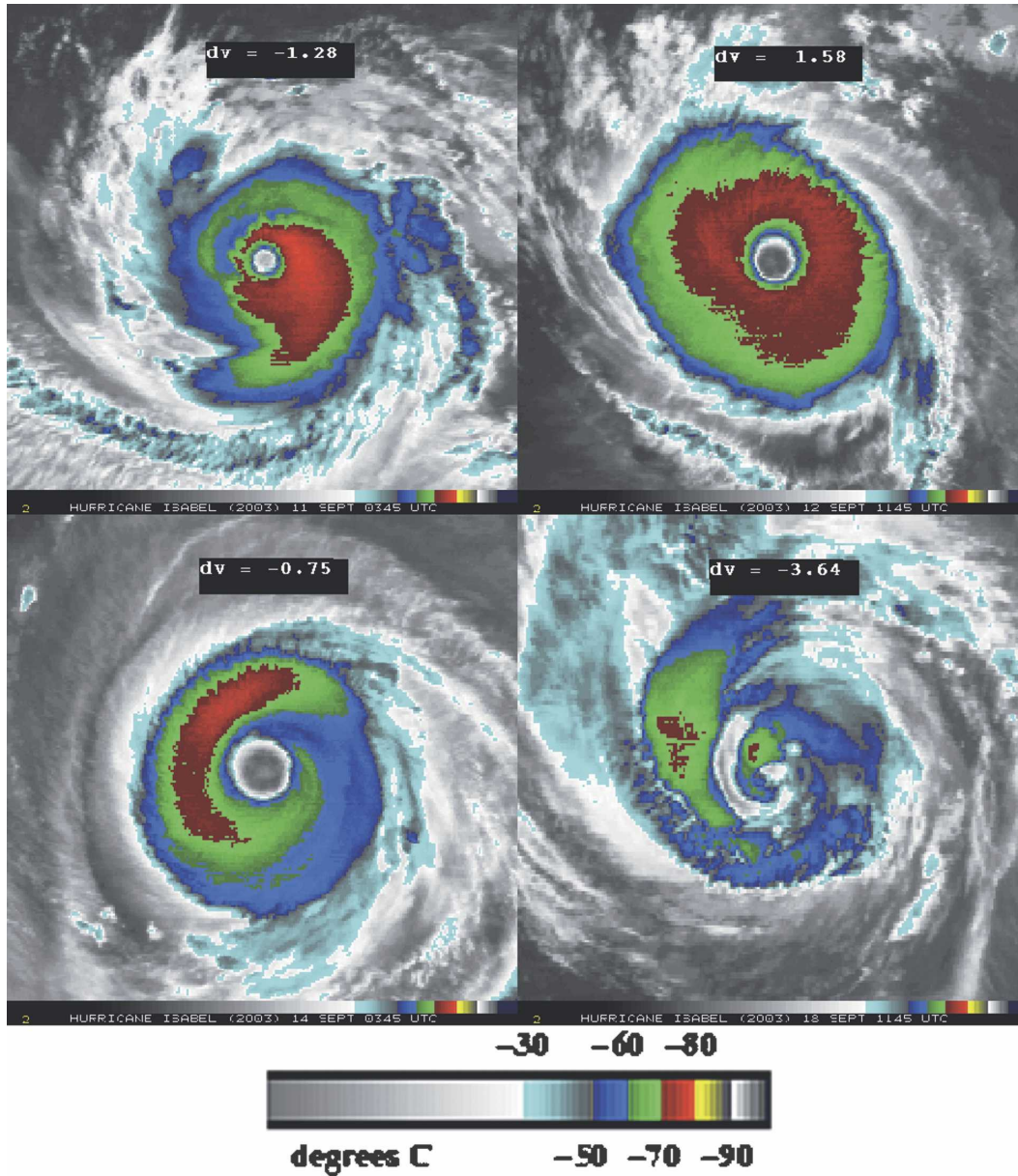


FIG. 5. Examples of GOES IR satellite imagery from Hurricane Isabel (2003) and corresponding discriminant function values ( $dv$ ) shown in the upper center of each panel. Results are based upon dependent data and negative values of  $dv$  discriminate AH cases. Imagery times are (top left) 0345 UTC 11 Sep, (top right) 1145 UTC 12 Sep, (bottom left) 0345 UTC 14 Sep, and (bottom right) 1145 UTC 18 Sep, and are also shown at the bottom of each panel.

UTC due to satellite eclipse times.<sup>1</sup> Notice that as Isabel changes from an asymmetric hurricane on 11 September to an AH on 12 September, the discriminant value goes from negative to positive. On 14 September

<sup>1</sup> Note that some recently launched operational geostationary satellites (i.e., *GOES-13*, *Meteosat-8*, and *Meteosat-9*) operate through the eclipse periods.

at 0345 UTC, following a separate annular period on 13 September through early on 14 September (not shown), the storm displays a distinct banding structure in the enhanced temperatures that wraps around the storm, instead of a more continuous ring of nearly constant temperatures, and thus is a NAH. The image on 18 September shows an example of an extreme NAH case. For these four images the environment is also varying, which also contributes to the estimate of the discrimi-

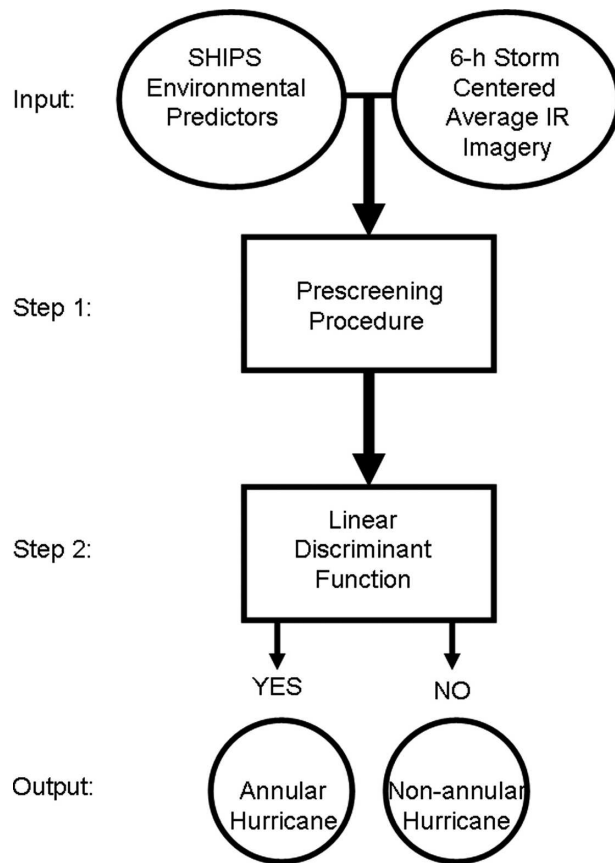


FIG. 6. Schematic of the two-step procedure used to objectively identify AHs.

nant value. The 200-hPa zonal winds were  $-6.7$ ,  $-3.0$ ,  $0.7$ , and  $-1.5 \text{ m s}^{-1}$  and the SSTs were  $28.4$ ,  $28.2$ ,  $28.4$ , and  $27.5^\circ\text{C}$ , in these images, respectively. During the period between 11 and 18 September, the algorithm properly (improperly) identified 8 (8) of the AH periods and 12 (0) of the NAH periods as Isabel went through four separate 12–14-h subjectively identified AH periods.

In summary, an algorithm to detect AHs is created using a two-step process. The first step is to prescreen the data using known environmental and storm-scale factors that are indicative of AHs. This step reduces the sample from 976 hurricane 6-h cases that have intensities greater than or equal to 85 kt to 241 cases that could be AHs. The second step is to create an LDA algorithm to identify AHs using the period 1995–2003, incorporating those remaining 241 six-hour cases. The output of the LDA, the discriminator function, is an objective measure of whether a storm is or is not an AH and how “annular” a particular case is. This two-step algorithm is illustrated schematically in Fig. 6 and is applied to independent data and tested in the next section.

TABLE 5. Normalized coefficients of the AH discriminant vector based upon the 1995–2006 AH cases. Variables as in Table 1. Note the discriminant divider is a unitless number that causes the discriminant function values to be centered about a zero value.

Discriminator	Mean	Std dev	Normalized coefficient
$\sigma_c$	4.23	2.45	-0.44
VAR	558.21	218.52	0.61
$\Delta T_{\text{eye}}$	56.73	21.61	0.81
U200	-4.55	2.89	-0.15
SST	27.68	1.04	-0.80
Discriminant divider			0.76

#### 4. Independent testing and final algorithm

The algorithm discussed in the previous section is tested using independent datasets collected during 2004–06. This involves applying the LDA coefficients shown in Table 4 to the SDD and IR satellite imagery results during those seasons, to objectively identify the AH periods shown in Table 2. During the years 2004–06 there were 2424 total 6-h cases of which 387 had intensities greater than 84 kt and 82 passed the prescreening process. Of these remaining 82 cases, 21 cases were objectively identified as AHs and 61 cases were identified as NAHs. Of the objectively identified AH cases, seven were associated with times listed in Table 2. Of the subjectively identified times 7 out of 7 were properly identified, leaving 14 false positive cases. Of the 14 false positive 6-h cases, only 3 were associated with Hurricane Jova of 2005, which never became an AH. The result of the 3-yr independent test is that the two-step objective AH identification scheme identified 100% of the AH cases with a false alarm rate of  $\sim 4\%$ , noting that there were 380 NAHs.

The results of the independent and dependent testing of the two-step objective AH identification scheme show that AHs can be identified objectively and in a real-time manner. With a goal of creating a real-time AH identification index, the next step is to use the entire dataset to estimate a final set of LDA coefficients. There were 1363 six-hour cases that had intensities greater than 84 kt, and screening produced 323 cases for the LDA. Table 5 shows the normalized parameter weights determined by the LDA, and the means and standard deviations of the 323 screened cases in the 12-yr sample (1995–2006). Comparing Tables 4 and 5, the addition of the 2004–06 cases has changed the weights in such a way that all of the variables except VAR have a larger influence on the discriminant function.

To more easily interpret the discriminant function, the discriminant values for annular hurricanes are

scaled from 0 to 100 so that a value of 0 indicates the answer “not an AH,” a value of 1 indicates the possibility of a AH with the least likelihood, and a value of 100 indicates an AH with the greatest likelihood. Discriminant values of  $-0.3$  and  $2.3$  correspond to scaled index values of 1 and 100, respectively, and scaled index values are also set to 0 and to 100 for discriminant function values less than (greater than) than  $-0.3$  and  $2.3$ , respectively. These values represent an objective degree of AH characteristics that are satisfied and should not be attributed to a probability. These threshold values were chosen to maximize the hit rate and minimize the false alarm rate based on information contained in the cumulative probability distributions of the dependent discriminant function values for the years 1995–2006. These values correspond to a  $\sim 96\%$  hit rate and a  $\sim 6\%$  false alarm rate in the developmental data, considering there are 1363 possible cases. Many ( $\sim 47\%$ ) of the false alarm cases were associated with storms that either were becoming AHs or had recently been AHs.

## 5. Summary and future plans

Annular hurricanes (AHs) are intense tropical cyclones with average intensities of approximately 110 kt and are potentially high-impact events when affecting coastal areas. With respect to intensity, AHs also are significantly stronger, maintain their peak intensities longer, and weaken more slowly than the average tropical cyclone. As a result, average official forecast intensity errors for these types of tropical cyclones were 10%–30% larger than the 5-yr (1995–99) mean official errors during the same period. While forecast errors associated with AHs have improved since 1999, underforecasting the intensity (i.e., too rapidly forecasting weakening) of these systems is still common. For these reasons, the identification of AHs in an operational setting could help improve tropical cyclone intensity forecasts by alerting forecasters that slower-than-average weakening of the current TC is likely to occur, especially if environmental conditions are forecast to remain fairly constant. Fortunately, the climatological distribution of AHs suggests that they are more likely in the tropics and well away from the U.S. mainland and may be more of a threat to the Windward, Leeward, and Hawaiian Islands; however, there is evidence that one case that is not included in this study, Hurricane Hugo, which made landfall near Charleston, South Carolina, in 1989, may have been an AH just before it went inland. Datasets to examine the Hurricane Hugo (1989) case are currently being collected.

This paper uses the information contained within

Knaff et al. (2003) and new knowledge about the structure of AHs gained from both idealized numerical simulations and new observations of tropical cyclones, to create an objective method of identifying AHs. The objective method uses information about the storm's environmental conditions, intensity, and appearance in IR satellite imagery via a two-step algorithm (see Fig. 6). The first step, prescreening, removes all cases that do not have the intensity and environmental characteristics associated with tropical cyclones. If the case passes the prescreening, it is then passed to a linear discriminant function, which uses five factors to estimate the degree to which a specific case is annular. To go one step further, the resulting linear discriminant value is then scaled from 0 to 100, where 0 indicates “not an annular hurricane” and values 1 to 100 indicate that the case is likely an AH, with larger values indicating greater confidence.

The algorithm described here was tested in a real-time operational setting at the National Hurricane Center during the 2007 hurricane season. Since then this algorithm has been operationally implemented within the SHIPS model framework and the AH index is provided as part of the text output of that model.

Although this algorithm is now available to hurricane forecasters, there are several research and product development studies that remain. Using past AH hurricane cases, an objective correction to the SHIPS and Statistical Typhoon Intensity Prediction Scheme (Knaff et al. 2005) intensity forecast models can be developed. Also, since AHs do exist in other basins [e.g., Typhoon Jelawat (2000) and Typhoon Saomai (2006) in the western North Pacific and Tropical Cyclone Dora (2007) in the South Indian Ocean], IR satellite imagery of tropical cyclones (e.g., Knapp and Kossin 2007) and high-quality reanalysis datasets could be used to objectively identify and document the climatology of AHs globally. Finally, since the environmental conditions of AHs, save the SST conditions, are also conducive for very strong tropical cyclones, research could be pursued to identify not only AHs but also those tropical cyclones that are likely to form secondary eyewalls, which is also a forecast problem. Secondary eyewall formation will more heavily utilize microwave imagery from low earth orbiting satellites to identify those time periods and storms that experience such events. This research has begun and results will be reported in due course.

*Acknowledgments.* This research is supported by NOAA Grant NA17RJ1228 through supplemental hurricane funding made available following the 2004 Atlantic hurricane season. The authors would also like to thank the three anonymous reviewers for their con-

structive and helpful comments. The views, opinions, and findings in this paper are those of the authors and should not be construed as an official NOAA and/or U.S. government position, policy, or decision.

## REFERENCES

- Bender, M. A., 1997: The effects of relative flow on asymmetric structures in hurricanes. *J. Atmos. Sci.*, **54**, 703–724.
- Chan, J. C. L., and R. T. Williams, 1987: Analytical and numerical studies of the beta-effect in tropical cyclone motion. Part I: Zero mean flow. *J. Atmos. Sci.*, **44**, 1257–1265.
- DeMaria, M., and J. Kaplan, 1994a: A Statistical Hurricane Intensity Prediction Scheme (SHIPS) for the Atlantic basin. *Wea. Forecasting*, **9**, 209–220.
- , and —, 1994b: Sea surface temperature and the maximum intensity of Atlantic tropical cyclones. *J. Climate*, **7**, 1324–1334.
- , and —, 1999: An updated Statistical Hurricane Intensity Prediction Scheme (SHIPS) for the Atlantic and eastern North Pacific basins. *Wea. Forecasting*, **14**, 326–337.
- , M. Mainelli, L. K. Shay, J. A. Knaff, and J. Kaplan, 2005: Further improvement to the Statistical Hurricane Intensity Prediction Scheme (SHIPS). *Wea. Forecasting*, **20**, 531–543.
- Fiorino, M., and R. L. Elsberry, 1989: Some aspects of vortex structure related to tropical cyclone motion. *J. Atmos. Sci.*, **46**, 975–990.
- Jarvinen, C., J. Neumann, and M. A. S. Davis, 1984: A tropical cyclone data tape for the North Atlantic basin, 1886–1983: Contents, limitations and uses. NOAA Tech Memo. NWS NHC 22, Coral Gables, FL, 21 pp. [Available from NTIS, 5285 Port Royal Rd., Springfield, VA 22161.]
- Kalnay, E., and Coauthors, 1996: The NCEP/NCAR 40-Year Reanalysis Project. *Bull. Amer. Meteor. Soc.*, **77**, 437–471.
- Knaff, J. A., and R. M. Zehr, 2007: Reexamination of tropical cyclone wind–pressure relationships. *Wea. Forecasting*, **22**, 71–88.
- , J. P. Kossin, and M. DeMaria, 2003: Annular hurricanes. *Wea. Forecasting*, **18**, 204–223.
- , R. M. Zehr, and M. DeMaria, 2005: An operational Statistical Typhoon Intensity Prediction Scheme for the western North Pacific. *Wea. Forecasting*, **20**, 688–699.
- , —, —, T. P. Marchok, J. M. Gross, and C. J. McAdie, 2007: Statistical tropical cyclone wind radii prediction using climatology and persistence. *Wea. Forecasting*, **22**, 781–791.
- Knapp, K. R., and J. P. Kossin, 2007: A new global tropical cyclone data set from ISCCP B1 geostationary satellite observations. *J. Appl. Remote Sens.*, **1**, 013 505.
- Kossin, J. P., 2002: Daily hurricane variability inferred from GOES infrared imagery. *Mon. Wea. Rev.*, **130**, 2260–2270.
- , J. A. Knaff, H. I. Berger, D. C. Herndon, T. A. Cram, C. S. Velden, R. J. Murnane, and J. D. Hawkins, 2007: Estimating hurricane wind structure in the absence of aircraft reconnaissance. *Wea. Forecasting*, **22**, 89–101.
- Kwok, J. H. Y., and J. C. L. Chan, 2005: The influence of uniform flow on tropical cyclone intensity change. *J. Atmos. Sci.*, **62**, 3193–3212.
- Lord, S. J., 1993: Recent developments in tropical cyclone track forecasting with the NMC Global Analysis and Forecast System. Preprints, *20th Conf. on Hurricanes and Tropical Meteorology*, San Antonio, TX, Amer. Meteor. Soc., 290–291.
- Maclay, K. S., 2006: A study of tropical cyclone structural evolution. M.S. thesis, Dept. of Atmospheric Sciences, Colorado State University, 110 pp. [Available from Atmospheric Branch, Morgan Branch, Colorado State University, Fort Collins, CO 80523.]
- Mason, S. J., and N. E. Graham, 1999: Conditional probabilities, relative operating characteristics, and relative operating levels. *Wea. Forecasting*, **14**, 713–725.
- Mueller, K. J., M. DeMaria, J. A. Knaff, J. P. Kossin, and T. H. Vonder Haar, 2006: Objective estimation of tropical cyclone wind structure from infrared satellite data. *Wea. Forecasting*, **21**, 990–1005.
- Peng, M. S., B.-F. Jeng, and R. T. Williams, 1999: A numerical study on tropical cyclone intensification. Part I: Beta effect and mean flow effect. *J. Atmos. Sci.*, **56**, 1404–1423.
- Reynolds, R. W., 1988: A real-time global sea surface temperature analysis. *J. Climate*, **1**, 75–86.
- Ritchie, E. A., 2004: Tropical cyclones in complex vertical wind shears. Preprints, *26th Conf. on Hurricanes and Tropical Meteorology*, Miami, FL, Amer. Meteor. Soc., 88–89.
- , and W. M. Frank, 2007: Interactions between simulated tropical cyclones and an environment with a variable Coriolis parameter. *Mon. Wea. Rev.*, **135**, 1889–1905.
- Wang, Y., and G. J. Holland, 1996a: The beta drift of baroclinic vortices. Part I: Adiabatic vortices. *J. Atmos. Sci.*, **53**, 411–427.
- , and —, 1996b: The beta drift of baroclinic vortices. Part II: Diabatic vortices. *J. Atmos. Sci.*, **53**, 3737–3756.
- , and —, 1996c: Tropical cyclone motion and evolution in vertical shear. *J. Atmos. Sci.*, **53**, 3313–3332.
- Wilks, D. S., 2006: *Statistical Methods in the Atmospheric Sciences*. 2nd ed. Academic Press, 467 pp.
- Wu, L., and S. A. Braun, 2004: Effect of convective asymmetries on hurricane intensity: A numerical study. *J. Atmos. Sci.*, **61**, 3065–3081.